Energy & Buildings 211 (2020) 109755

Contents lists available at ScienceDirect

Energy & Buildings

journal homepage: www.elsevier.com/locate/enbuild

Sorbent based enthalpy recovery ventilator

Ecem Cerrah, Claire McCague, Majid Bahrami*

Laboratory for Alternative Energy Conversion (LAEC), School of Mechatronic Systems Engineering, Simon Fraser University, 250-13450 102 Avenue, Surrey, BC V3T 0A3, Canada

ARTICLE INFO

Article history:
Received 27 June 2019
Revised 2 December 2019
Accepted 3 January 2020
Available online 7 January 2020

Keywords:
Heat/enthalpy recovery ventilator
Sorption composites
Cold climate
De/humidification
Boundary layer interruption

ABSTRACT

A novel concept – disc type sorbent based enthalpy recovery ventilator (SERV) – is presented for the first time. The proposed SERV is a compact system that includes two separate sections for vapor and heat recovery, has low pressure drop, and eliminates frozen exhaust issue that affects the performance of conventional heat and enthalpy recovery ventilators in cold climates. A new theoretical model is developed for the heat and mass transfer in the air channels of the sorbent discs. A sensitivity analysis is performed to design the main parameters, e.g. channel diameter and spacing, to achieve optimum performance. A prototype SERV is built and tested in a custom-made experimental set-up designed based on ASHRAE 84 standards. The performance of SERV is evaluated for several air flow rates (3–18 CFM), cycle times, and outdoor air temperatures down to -15 °C. The SERV prototype – consisting of 2.1 kg of active sorbent material and 2 kg of heat storage materials –recovered up to 70% of heat and 80% of moisture from exhaust air with 60% less pressure drop relative to measured comparable systems in the literature.

Abbreviations

RD	Regular density
RH	Relative humidity
MRC	Moisture recovery capacity, kg/h
MRC*	Modified moisture recovery capacity, kg water/kg sorbent * hour
RPH	Revolution per hour
VCOP	Ventilation coefficient of performance

1. Introduction

The building sector accounts for 40% of global energy consumption and 18% of GHG emissions [1]. The global energy demand of buildings is predicted to increase from 145 EJ in 2013 to 243 EJ by 2050 [2,3]. In Canada, due to the cold climate, space heating accounts for 61% of the residential energy consumption [4]. International Energy Agency (IEA) estimates a 53% reduction in the energy demand by 2050 can be achieved through implementation of building codes with far more stringent targets than the current ones, i.e., improving the air-tightness, insulation, and the energy efficiency of household appliances [5]. Improving the air-tightness increases the need for mechanical ventilation to keep the human comfort per ASHRAE standards [6]. In northern climates, such as Canada, Russia, and Northern Europe, the fresh air driven into buildings should be heated and humidified. Heat/enthalpy recovery ventilators (HRV/ERVs) can be used to reduce the energy consumption. As per ATTMA standard L1, the air tightness of a building is measured in air changes per hour at a pressure differential of 50 Pascals (ACH_{50}) [7]. Air-tight buildings with an infiltration rate of 2.5 ACH_{50} equipped with enthalpy recovery ventilators (ERVs) can operate in a cost-effective manner compared to conventional buildings (7 ACH_{50}) saving 20 to 40% of heating costs in different regions of Canada [8].

HRVs can recover 60–95% of the heat, depending on the heat exchanger performance and climate conditions [9]. In cold climates (below 0 °C), the energy savings are more significant. However, there are limitations for HRV operation for high moisture content of the exhaust air that can lead to frost formation in the exhaust, as seen in Fig. 1 [10,11]. Desiccant coated wheels or membrane based ERVs that recover both heat and moisture from the exhaust air, operate with a lower frosting limit, down to −10 °C, compared to conventional HRVs [12].

Beattie et al. [11] tested a polypropylene based HRV, a polymerized paper based ERV and two different membrane type ERVs (provided by dpoint Technologies) with outdoor temperatures between −5 to −35 °C. In all tested systems frost problem was observed at operation below −10 °C outdoor temperature. They reported 20% to 30% of air flow reduction due to ice formation in membrane based ERVs and HRV after 2 h of operation. With factory set defrost strategy HRV had the highest sensible effectiveness (~0.84)

* Corresponding author.
E-mail addresses: ecerrah@sfu.ca (E. Cerrah), mbahrami@sfu.ca (M. Bahrami).

https://doi.org/10.1016/j.enbuild.2020.109755
0378-7788/

Nomenclature

A_{cs}	Cross-sectional area for air flow, m^2
As	Cross-sectional area of the sorbent layer flow, m^2
$c_{p,a}$	Air specific heat, J/kgK
$c_{p,s}$	Sorbent specific heat, J/kgK
C_1	Constant number
C_2	Constant number
C_3	Constant number
C_4	Constant number
d	Channel diameter, m
D	Disc diameter, m
D_a	Gas diffusivity of air-vapor mixture, m^2/s
dz	Infinitesimal length, m
f	Friction factor
h	Convective heat transfer coefficient, W/ m^2K
h_m	Convective mass transfer coefficient, kg/ m^2s
k_a	Thermal conductivity of the air, W/mK
L	Channel length, m
M_s	Mass of the sorbent, kg
$\dot{m}$	Mass flow rate
n	Number of cycles
Nu_H	Nusselt number for constant heat flux
Nu_T	Nusselt number for constant temperature
Pr	Prandtl number
P_{vs}	Saturation pressure of the vapor in air, Pa
$\dot{q}$	Heat transfer rate
$\dot{Q}_{heater}$	Heating power, W
s	error
Sh	Sherwood number
S_{BET}	Brunauer-Emmett-Teller Surface area, m^2/g
t	Time, s
T	Temperature, °C
u	Air velocity, m/s
$\dot{V}_a$	Air volumetric flow rate, m^3/h
x	Coordinate
X_s	Water uptake in the sorbent, g_w/g_s
z	Coordinate

Greek symbols

α	Thermal diffusivity, m^2/s
β	Degree of humidification
δ	Thickness of the desiccant layer, m
$\in$	Aspect ratio
ε	Porosity
ΔH	Adsorption heat, J/kg
γ	Shape factor
ΔP	Pressure drop, Pa
ρ	Density, kg/m^3
ω	Specific humidity, g_w/kg_{air}

Subscripts

a	air
BU	between units
EA	exhaust air
m	mass
OA	outdoor air
RA	return air
s	sorbent
SA	supply air
w	water

and the ERVs had about 0.76–0.78. Latent heat transfer effectiveness was 0.61 for the polymerized paper based ERV and 0.46 and 0.52 for membrane based ERVs at −25 °C outdoor temperature. At extreme cold climates (below −10 °C) potential for energy savings due to heat recovery increases; however need for a defrost mechanism costs an energy penalty and complexity.

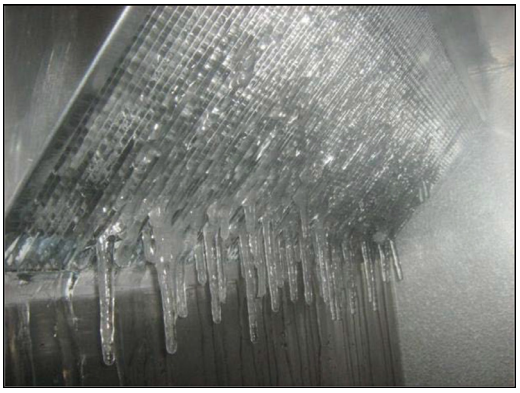

Fig. 1. Frost formation at the exhaust of an ERV [10].

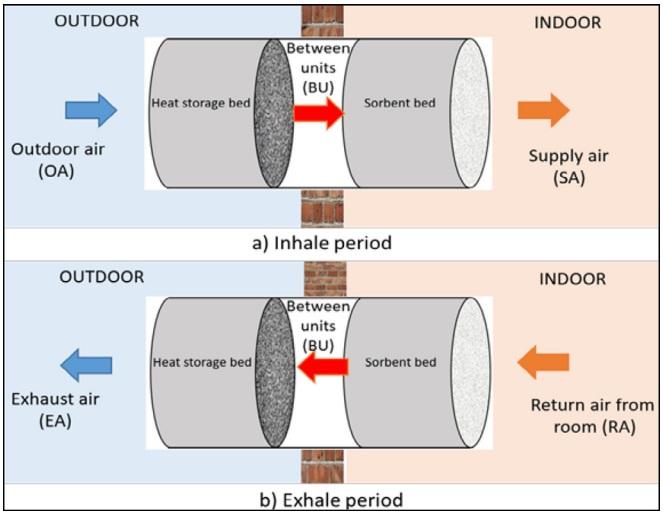

Fig. 2. Intermittent operation, "inhale" and "exhale" of air streams, in VENTIREG and SERV.

Recently, a new enthalpy recovery ventilation system, named VENTIREG [13], was built and tested in Novosibirsk, Russia (winter temperature down to −30 °C). In this system, heat recovery and moisture recovery were performed by separate packed beds consisting of sorbent material, i.e., silica gel, alumina and alumina impregnated with $CaCl_2$ (pellet size 1.8–4.5 mm in diameter and 6–8 mm in length) and heat storage material, glass balls, lead balls (of 2–4.5 mm diameter) or gravels (irregular shape 4–7 mm in size). Laboratory and field tests of the system demonstrated 70–90% moisture recovery and 60–96% heat recovery from outlet to inlet air streams [13,14]. VENTIREG's only operating cost was fan electric power, reported to be 20–40 W for a prototype supplying 80 CFM of fresh air.

The VENTIREG operates in intermittent inhale and exhale periods as schematically shown in Fig. 2. Due to its high moisture recovery performance, VENTIREG does not have frost issue for the tested conditions, down to −35 °C. It was mentioned that scaling up of this system for larger applications may lead to a decrease in efficiency; therefore, mathematical modeling is required to optimize the bulky packed bed design [13]. For VENTIREG's packed bed design, the developing region is negligible and both temperature and vapor concentration profiles should be considered as fully developed regions [15]. In the entrance region, where the temperature and concentration profiles are developing, the heat and mass

transfer coefficients are much higher compared to the fully developed region [16]. Interrupting boundary layer is a well-known approach to postpone the boundary layer development to increase heat/mass transfer [17].

In the present study, a novel compact disc-type sorbent enthalpy recovery ventilator (SERV) is proposed to increase heat/mass transfer coefficients, reduce sorbent materials, and reduce the needed fan power. The proposed SERV includes separate vapor (disc-type sorption composite) and heat recovery (gravel) sections and a fan to circulate the air and operates intermittently similar to VENTIREG, see Fig. 2. The vapor recovery section consists of 5 composite sorbent discs made of $CaCl_2$, mesoporous silica gel, and PVP 40, 2.5 kg in total. The heat recovery section is packed with 2 kg of aquarium gravel. Multiple discs, featuring air channels, with spacing in between, are used to interrupt the thermal and concentration boundary layer development, thus enhancing heat and mass transfer coefficients. A theoretical model is developed to guide the design of the sorbent discs and SERV prototype. The sorbent discs are built and tested in a custom built experimental set-up in our laboratory, as per ASHRAE standard 84 [18]. The de/sorption performance is notably improved in the proposed SERV, due to enhanced heat and mass transfer properties, high uptake properties of the composite sorbent and air channels that reduce the pressure drop compared to packed bed design.

2. Theoretical model

A front view of the sorbent disc with identical air channels and side view of a unit channel with air/sorbent control volumes are shown schematically in Fig. 3. Air and sorbent control volumes are connected by heat and mass transfer through the air/sorbent interface. The conservation of energy and concentration of water vapor equations should be solved to predict the transient temperature and moisture concentration of air and sorbent layer throughout the air channels. During the inhale period, the air stream at the inlet of the channel, return air (*RA*), is dehumidified as it flows through the channels. Air leaves the channels as exhaust air (*EA*) with less water vapor content. During the exhale period, dry outdoor air (*OA*), assumed to have recovered the heat in heat storage bed enters the channel at the opposite inlet of the channel, recovers the water vapor stored in the sorbent walls during the previous inhale period. Cycle time-averaged temperature and moisture concentration of air at the outlet of the channel indicates the *EA* and *SA* conditions of the sorbent bed, respectively. During experiments at least 15 cycles performed before taking measurements and mass balance is ensured between inhale / exhale cycles.

The assumptions used to develop the present model are:

- All air channels on the discs are identical; therefore heat and mass transfer in a unit channel is modeled as a representative of the entire disc, see Fig. 3. The outlet air condition is considered as the inlet air conditions for the successive disc.

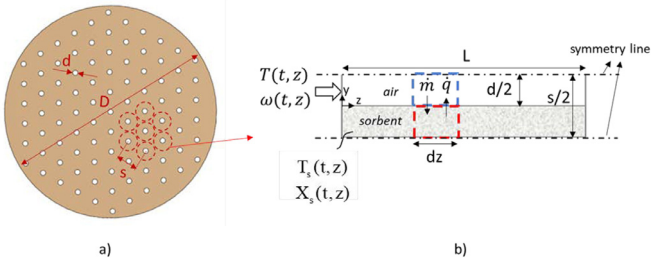

Fig. 3. a) Air channels on sorbent disc, b) air and sorbent control volumes are shown on a unit channel of the sorbent disc.

- Laminar flow is assumed in the channel because the Reynolds number is less than 2,300. Both for modeling and experimental study, air velocity in the unit channels are between 1.5 to 3 m/s, which leads to Reynolds number in the range 507- 1015, ensuring laminar flow assumption.
- The heat and mass transfer in the unit channel is modeled using bulk mean temperatures and moisture concentrations of the air (mean bulk temperature and moisture concentration are assumed for air flow within each discrete dz element, shown in Fig. 3b.) [19,20]
- Thermal boundary layer and concentration boundary layer develop simultaneously as the Lewis number is approximately one [19,21]. This assumption is used to calculate the convective mass transfer coefficient (h_m) from the convective heat transfer coefficient (h).
- The axial heat conduction and mass diffusion are neglected (z-direction) in both air and desiccant control volumes [19].
- Thermophysical properties of dry air and dry desiccant are constant, bulk properties are functions of moisture content only.

2.1. Performance matrices

Latent effectiveness, ε_L, and moisture recovery capacity (MRC) are often used to evaluate the moisture recovery performance of de/humidification systems, and are defined as:

$$\varepsilon_L = \frac{\omega_{SA} - \omega_{OA}}{\omega_{RA} - \omega_{SA}} \tag{1}$$

and

$$MRC = \dot{m}_a(\omega_{SA} - \omega_{OA}) \tag{2}$$

where $\dot{m}$ is the air mass flow rate in kg/s, and the ω is the specific humidity ratio (kg_{water}/kg_{air}).

These parameters do not represent compactness and the fan power consumption, which is the only operating system cost. In this study, a new parameter, ventilation coefficient of performance (VCOP), and non-dimensionalized moisture recovery capacity (MRC*) are presented to evaluate the performance.

$$VCOP = \frac{\dot{m}_a(h_{SA} - h_{OA})}{\dot{V}_a \Delta P + \dot{m}_a(h_{RA} - h_{SA})} \tag{3}$$

$$MRC^* = \frac{\dot{m}_a(\omega_{SA} - \omega_{OA})}{M_S} \tag{4}$$

where h is the enthalpy of moist air in J/kg, M_s is the active sorbent mass (kg). The fan power consumption is expressed due to the pressure drop ΔP(Pa) and $\dot{V}_a$ (m^3) the volumetric flow rate.

$$\beta = \frac{\omega_{SA} - \omega_{OA}}{\omega_{RA}} \tag{5}$$

Degree of humidification (β) is defined to represent the amount moisture desorbed from the adsorbent with respect to the amount of moisture ejected from the room [14].

2.2. Governing equations

Conservation of mass and energy laws are applied to the control volume shown in Fig. 3b, and the following set of governing equations are derived based on the previous studies on heat and mass transfer at air-sorbent interfaces [19,22–27]:

$$\text{Air, mass conservation} \quad \rho_a A_{cs}\frac{\partial \omega_a}{\partial t} + u\rho_a A_{cs}\frac{\partial \omega_a}{\partial z} + h_m \pi d(\omega_a - \omega_s) = 0 \tag{6}$$

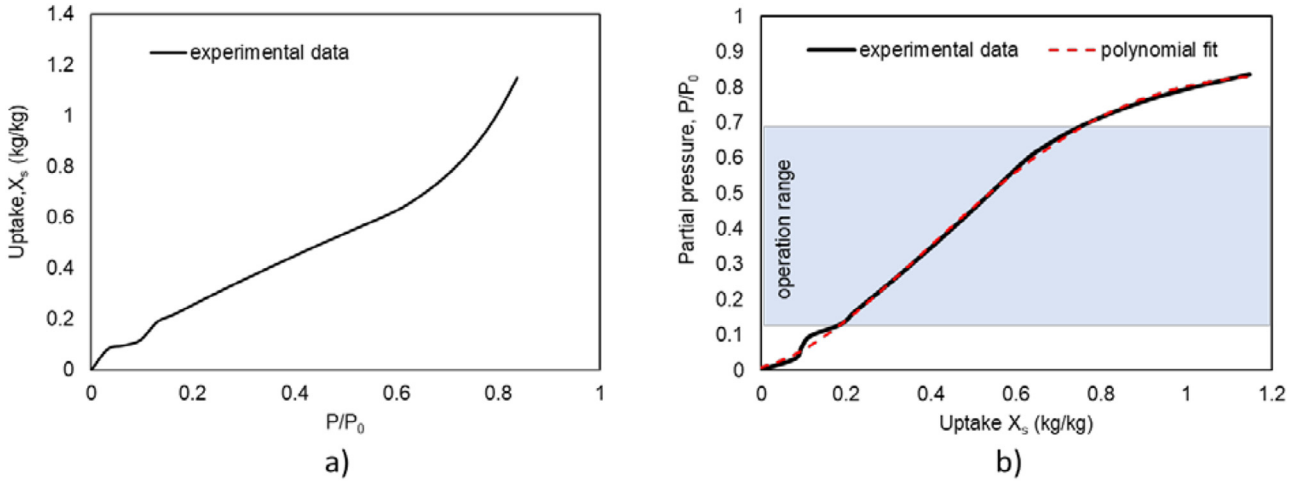

Fig. 4. a)$CaCl_2$- silica gel composite isotherm, and polynomial fit shown on the reversed axis for the range of operation.

$$\text{Sorbent, mass conservation} \quad A_s dz\left[\rho_s \frac{\partial X_s}{\partial t}\right] + h_m d\pi\, dz(\omega_s - \omega_a) = 0 \tag{7}$$

where u, ρ_a, ω_a are the velocity, density and specific humidity of the air, ω_s is the equivalent specific humidity in the sorbent, respectively. Channel cross-sectional area A_{cs} and the channel diameter d are geometrical parameters. h_m is the convective mass transfer coefficient for the air-sorbent interface. In the sorbent control volume; A_s is the cross-sectional area of the sorbent layer, ω_s (g/g dry air) is specific humidity in the pore volume in gas form and X_s (g/g sorbent) is the water uptake in the sorbent material, respectively.

Energy balance in air and sorbent control volumes are written in Eqs. (8 and 9):

$$\text{Air, energy conservation} \quad \rho_a c_{p,a} A_{cs}\frac{\partial T_a}{\partial t} + u\rho_a c_{p,a} A_{cs}\frac{\partial T_a}{\partial z} + h\pi d(T_a - T_s) = 0 \tag{8}$$

$$\text{Sorbent, energy conservation} \quad \rho_s c_{p,s} A_s \frac{\partial T_s}{\partial t} - h\pi d(T_a - T_s) - \rho_{s,dry} A_s \frac{\partial X_s}{\partial t}\Delta H_{ads} = 0 \tag{9}$$

In the sorbent wall, there is an additional source term to account for heat source/sink due to the heat of adsorption (ΔH_{ads}).

By means of psychometric relations, vapor partial pressure (P/P_0) in the sorbent can be used to calculate specific humidity in the sorbent (ω_s), where saturation pressure (P_{vs}) is a function of sorbent temperature:

$$\omega_s = \frac{0.62188(P/P_0)}{\left(\frac{P}{P_{vs}} - \frac{P}{P_0}\right)} \tag{10}$$

$$P_{vs} = e^{(23.196 - 3816.44/(T_s - 46.13))} \tag{11}$$

Water sorption isotherm of the $CaCl_2$-silica gel composite is measured using a thermogravimetric analyzer (IGA-002, Hiden Isochema) and the isotherm is plotted in Fig. 4a. As shown in Fig. 4b, a 4th order polynomial was fitted to the reversed axis isotherm data to express a correlation between vapor partial pressure (P/P_0) with water uptake (X_s):

$$\frac{P}{P_0} = 0.0086 + 0.2824X_s + 2.4271{X_s}^2 - 2.7958{X_s}^3 + 0.8803{X_s}^4 \tag{12}$$

Table 1
Coefficients based on boundary conditions and channel shape [28].

Coefficients based on boundary conditions		
Uniform wall temperature	C_3=0.409, C_1=3.24	$f(\mathrm{Pr}) = \frac{0.564}{[1+(1.664\mathrm{Pr}^{1/6})^{9/2}]^{2/9}}$
Uniform heat flux	C_3=0.501, C_1=3.86	$f(\mathrm{Pr}) = \frac{0.886}{[1+(1.664\mathrm{Pr}^{1/6})^{9/2}]^{2/9}}$
Coefficients based on channel shape		
$\gamma = 1/10$	C_2=1	C_4=1

2.3. Heat and mass transfer coefficients

Muzychka and Yovanovich [28,29] developed an analytical model that predicts Nusselt number (Nu) for combined entrance region by combining the asymptotic results for laminar boundary layer flow and Graetz flow for the thermal entrance region (L_t). Using the square root of the channel cross-sectional area as the characteristic length, solutions for similar geometries collapse onto a single curve, friction coefficient (fRe) and local Nu can be calculated as a function of aspect ratio ($\in$), and shape parameter (γ):

$$f\mathrm{Re}_d = \left[\left(\frac{12}{\sqrt{\in}(1+\in)\left[1 - \frac{192\in}{\pi^5}\tanh\left(\frac{\pi}{2\in}\right)\right]}\right)^2 + \left(\frac{3.44}{\sqrt{z^+}}\right)^2\right]^{1/2} \tag{13}$$

$$Nu(z^*) = \left[\left(\frac{C_4 f(\mathrm{Pr})}{\sqrt{z^*}}\right)^m + \left(\left\{C_2C_3\left(\frac{f\mathrm{Re}}{z^*}\right)^{1/3}\right\}^5 + \left\{C_1\left(\frac{f\mathrm{Re}}{8\sqrt{\pi}\in^\gamma}\right)\right\}^5\right)^{m/5}\right]^{1/m} \tag{14}$$

$$L_t = 19.80\left(\frac{C_2C_3}{C_1}\right)^3 \in^{1+3\gamma}(1+\in)^2\left[1 - \frac{192\in}{\pi^5}\tanh\left(\frac{\pi}{2\in}\right)\right]^2 \tag{15}$$

The constants based on the boundary conditions, air properties and channel shape are presented in Table 1.

At the sorbent air interface, neither heat flux nor the temperature of the sorbent wall is constant. Therefore, an averaged Nusselt number is used to estimate the convective heat transfer coefficient

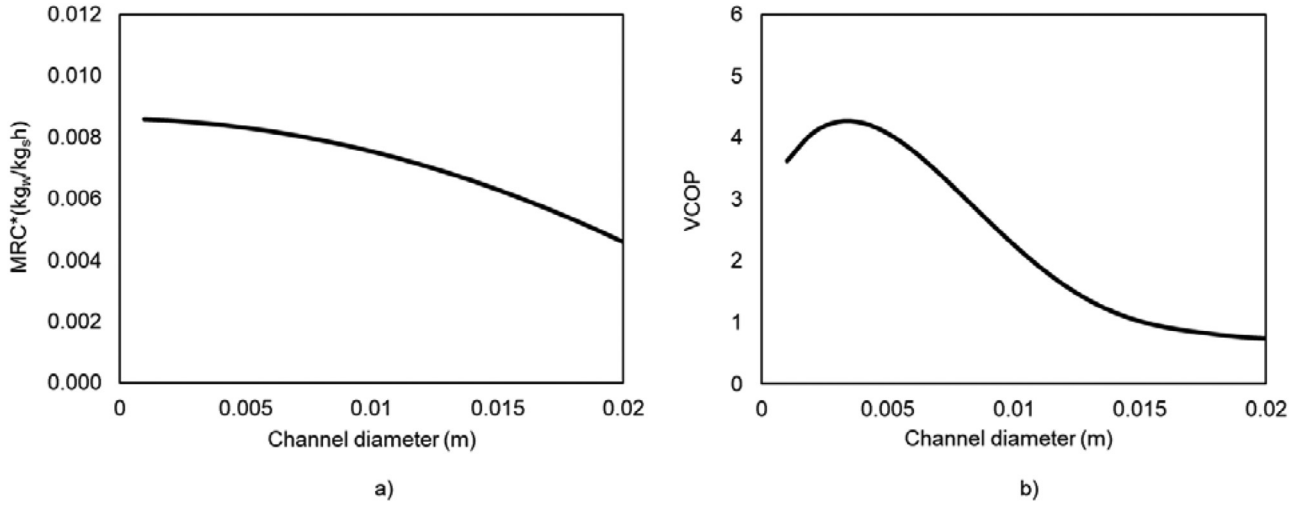

Fig. 5. Parametric study for the effect of channel diameter on SERV performance in terms of a) MRC*, b) VCOP.

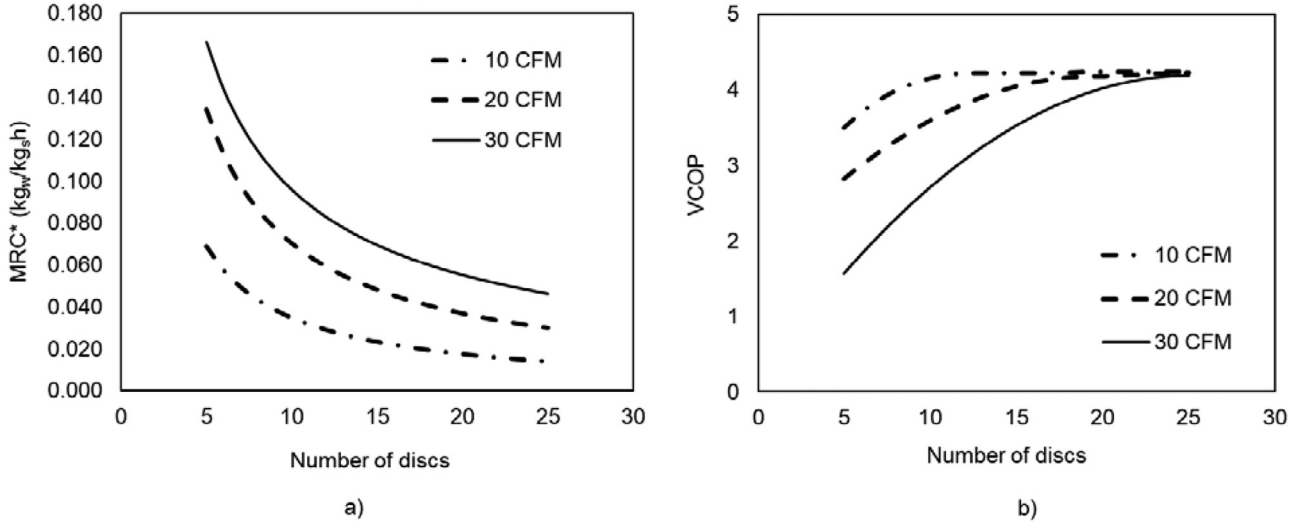

Fig. 6. Effect of number of discs on the performance in terms of a) MRC*, b) VCOP.

(h).

$$Nu = \frac{Nu_T + Nu_H}{2} \tag{16}$$

$$h = k_a Nu / d_h \tag{17}$$

Energy, mass and momentum equations in laminar boundary layer are similar. Reynolds analogy that is used to link the heat transfer coefficient (h) to friction factor (f) can be extended for mass transfer [30]. Mass transfer coefficient (h_m) can be related to heat transfer coefficient (h) by Lewis number (Le) which is the ratio of thermal diffusivity (α) to mass diffusivity (D_a). For air, the Lewis number is close to 1, therefore Sherwood number is equal to Nusselt number and following relation can be written [19]:

$$h_m = \frac{h}{\rho_a c_{p,a} Le^{2/3}} \tag{18}$$

where, gas diffusivity of air-vapor mixture, D_a is calculated using the following relation [25]

$$D_a = 2.302 \frac{P_0}{P} \left(\frac{T}{T_0}\right)^{1.81} 10^{-5} \tag{19}$$

2.4. Initial and boundary conditions

At both ends of the desiccant channel, shown in Fig. 3, insulated and impermeable boundaries are considered [9]:

$$\frac{\partial T_a}{\partial z} = \frac{\partial \omega_a}{\partial t} = 0, \text{at} x = 0, L \tag{20}$$

Periodic process and regeneration air conditions are applied as inlet conditions with the reversed flow direction. T_{RA} and ω_{RA} are return air inlet temperature and specific humidity; T_{OA} and ω_{OA} are outdoor air inlet conditions and n represent the number of cycles.

$$\begin{matrix} T_a = T_{OA} \\ \omega_a = \omega_{OA} \end{matrix} \text{att} = 0 + \text{nt}_{\text{cycle}} \tag{21}$$

$$\begin{matrix} T_a = T_{RA} \\ \omega_a = \omega_{RA} \end{matrix} \text{att} = \text{t}_{\text{inhale}} + \text{nt}_{\text{cycle}} \tag{22}$$

Coupled energy and mass balance equations are discretized along the disc thickness using a finite element method. Mathematical equations are written and solved in Matlab 2018a. Four partial differential equations (energy and mass balance equations) along with the desiccant isotherm equation are solved for five variables (T_a, T_d, ω, ω_s, X_s) using 4th order Runge-Kutta iteration method.

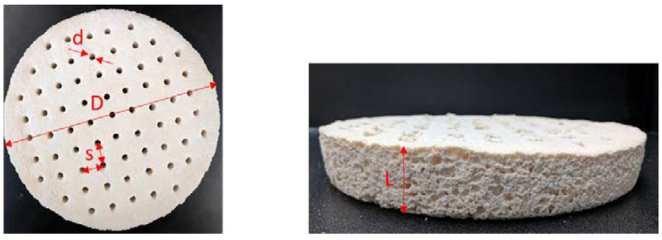

Fig. 7. Sorbent disc geometry, $d = 5$ mm, $s = 22$ mm, $D = 203$ mm, $L = 27$ mm.

Table 2
Constant design parameters for sensitivity analysis.

Disc diameter (D)	203.2 mm (8″)
Disc thickness (L)	25 mm
Return air temperature (T_{RA})	22 °C
Return air specific humidity (ω_{RA})	8.6 g_w/kg_a
Outdoor air temperature (T_{OA})	−10 °C
Outdoor air specific humidity (ω_{OA})	1 g_w/kg_a
Between units temperature (T_{BU})	13 °C
Half cycle time ($t_{halfcycle}$)	60 s
Air velocity in the channel (u_a)	2.5 m/s

3. Parametric study

A preliminary parametric study was performed using the above theoretical model. The diameter of the disc is chosen as a constant design parameter, 8″, considering the size of the experimental set-up built in our laboratory and the available size of molds to build the discs.

The performance of sorbent discs with air channel diameter varying from 2.5 mm to 20 mm is studied and plotted in Fig. 5. The air velocity per channel was kept constant, 2.5 m/s, by decreasing the number of channels as the channel diameter increased [31]. The constant parameters are listed in Table 2. The total air-sorbent surface area (A_s) in the channels is the largest for the design with the smallest size and highest number of channels, 3.5 cm^2. A_s decreases as the channels size increase and the number of channels decrease. The smallest A_s for this study is 0.25 cm^2 for the 20 mm diameter channel design. As shown in Fig. 5, the MRC* decreases with an increase in channel diameter due to a decrease in the number of channels and A_s. The effect of pressure drop is included in VCOP calculation as fan power. As expected, VCOP has a maximum (for 5 mm channel diameter) that indicates an optimum moisture recovery that is achieved with minimal fan power.

Due to manufacturing limitations, for this study, the average disc thickness (L) is measured 27 mm for all the designs, which is shorter than the entrance length (L_t) calculated by Eq. (15) above. The overall thickness of the sorbent discs unit is determined by the number of the sorbent discs. The increase in the number of discs is investigated in terms of MRC* and VCOP (see Fig. 6), for

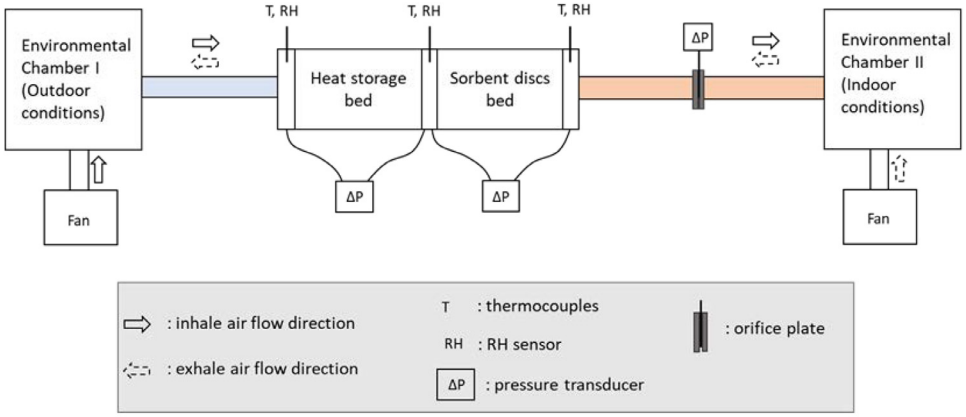

a)

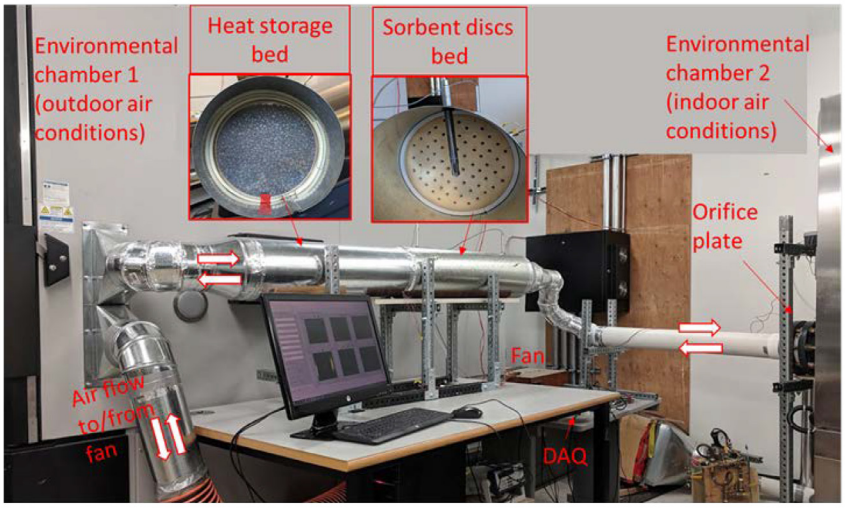

b)

Fig. 8. a) Schematic of the testbed, b) photo of the custom-built testbed in our laboratory.

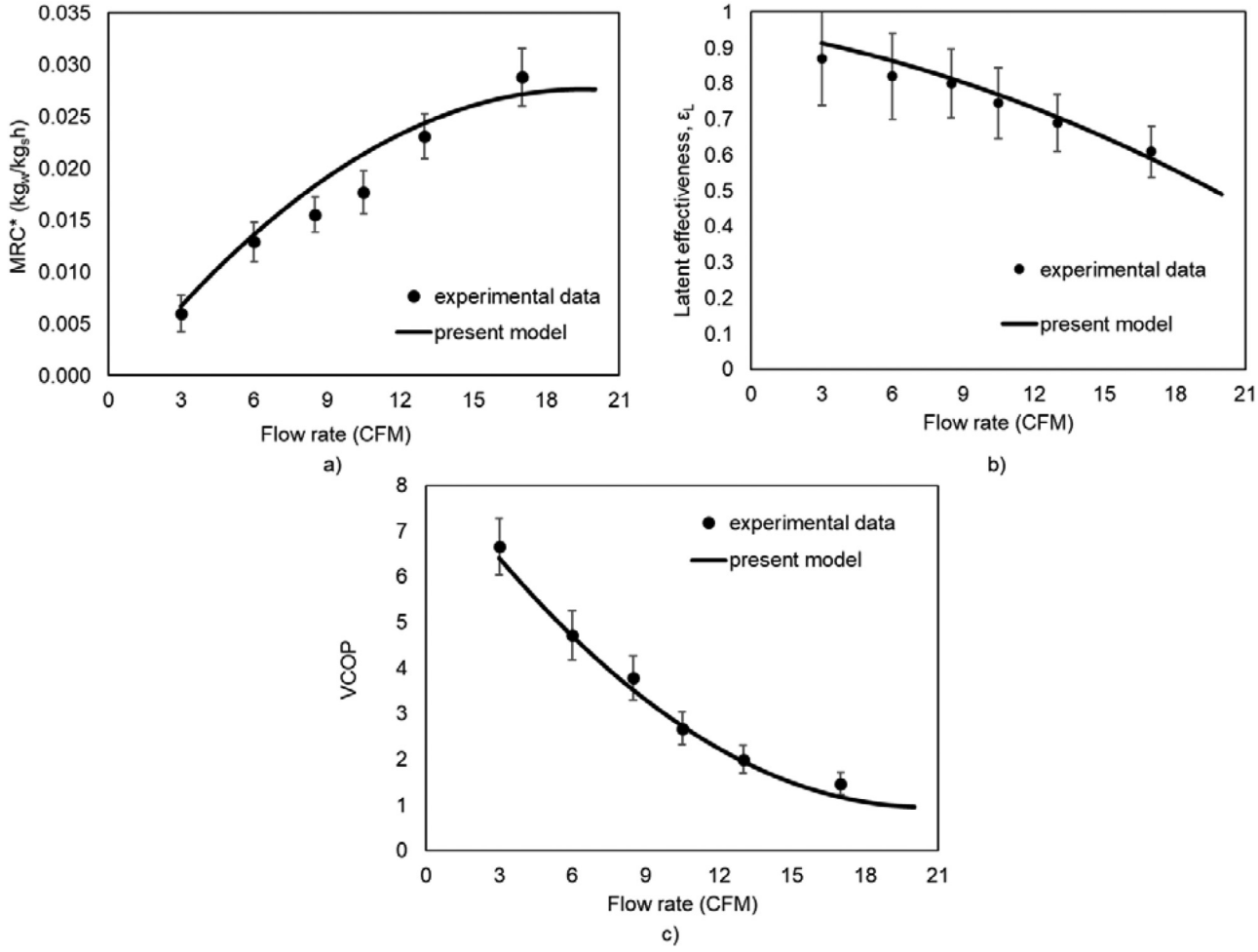

Fig. 9. Performance of the SERV at various air flow rates a) MRC*, b) ε_L, c) VCOP.

three different air flow rates, 10, 20, 30 CFM. At higher flow rates, the sorbent discs are in contact with a higher amount of moisture, therefore, there is a higher potential for moisture uptake. However, the increase in the total mass of the discs is larger than the increase in the moisture uptake, therefore, MRC* decreases.

The laboratory scale experimental set-up is designed to test the performance of SERV for up to 20 CFM. For the sorbent discs unit built with 5 discs, the VCOP drops about 15% as the air flow rate increases from 10 to 20 CFM. When the number of discs increases, the VCOP at different flow rates approaches its maximum. However, the increase in the total mass of the sorbent results in a decrease in MRC*. Therefore, about 15% decrease in VCOP is found tolerable, and 5 sorbent discs are built for the laboratory scale tests.

4. Sample preparation and experimental set-up

The sorbent disc is comprised of 55 wt% mesoporous silica gel (SiliaFLASH B150, Silicycle Inc.), 30 wt% $CaCl_2$ and 15 wt% polyvinylpyrrolidone (PVP) binder (40,000 MW, Sigma-Aldrich). Water was added to the combined materials to prepared a slurry that was poured into an aluminum baking container. The air channels were formed by inserting 69 glass rods of 5 mm in diameter. The mixture was oven dried and cured with three temperature steps, 80, 120, and 150 °C. The geometrical features of a sorbent disc is shown on Fig. 7. Each disc weighed 516 ± 15 g and had a density of 616 ± 19 kg/m^3. The macroporous structure of the discs can be observed in the side view in Fig. 7. During the drying process the $CaCl_2$ is deposited in the mesopores in the irregular-shaped grains of silica gel (0.2–0.5 mm). The vapor released during drying contributes to the creation of intergranular pores throughout the disc.

Nitrogen adsorption isotherms were measured with an Autosorb iQ-MP (Quantochrome Instruments) shown in Fig. 4a in the modelling section. Porosimetry for micropores and mesopores were measured by nitrogen porosimetry. The pore volume of the composite calculated from the nitrogen adsorption isotherm was 0.4434 cc/g (P/P_0 0.976, pores with radius < 41.7 nm). The BET (Brunauer, Emmett and Teller) the specific surface area (S_{BET}) of the composite was 103.613 m²/g with a mean pore diameter of 171 Å.

The sorbent discs featuring air channels were mounted in a custom-built test bed as shown in Fig. 8 and tested as per ASHRAE 84 standards [18] to measure the performance of the proposed SERV. An environmental chamber (Thermotron© Model XSE-3000–10–10) was used to supply outdoor air down to −15 °C, 80% RH up to 30 CFM. Indoor air condition, 20–22 °C and 35–50% RH, was prepared and supplied in the second environmental chamber (ESPEC© Model EPX-H2). Inhale and exhale air streams were supplied by two intermittently operating fans (Airflow Measurement Systems Inc.) connected to each environmental chamber. Voltage regulators were connected to the fans to adjust the flow rates in each air stream. The air was driven to the environmental chamber, passed through the test section and reached to the environmental

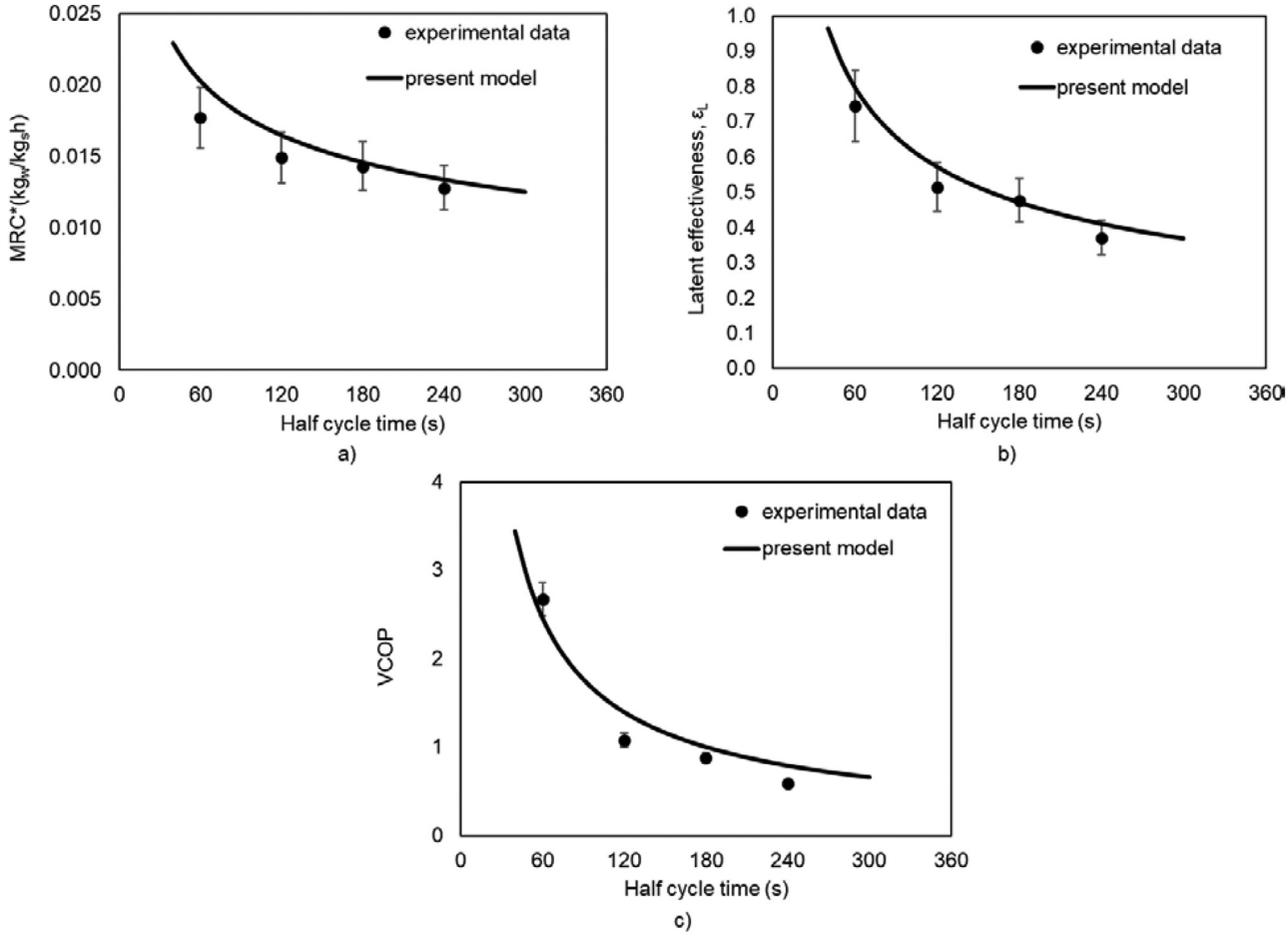

Fig. 10. Performance of the SERV for various half cycle times a) MRC*, b) ε_L, c) VCOP.

chamber at the other end. In the second half cycle, the flow was reversed by operating the second fan. Air flow and pressure drop were measured with an orifice plate (4″ Oripac© model 4150) and a differential pressure transducer (Setra Model 267), respectively. The test bed had two RH sensors (Vaisala, HUMICAP® HMP110) and twelve T-type thermocouples (Omega Engineering). The heat storage bed consisted of 2 kg of aquarium gravels in an 8″ diameter circular duct held by metal meshes.

5. Performance analysis

5.1. Flow rate variation

The flow rate of the air, passing through the sorbent bed is one of the most critical parameters that affect the performance of SERV. Similar to membrane or desiccant wheel type ERVs, SERV should be sized based on the minimum required air flow rate. For the sorbent discs placed in the test set-up, a set of experiments were performed with air flow rate varying from 6 to 17 CFM. In all the tests, the indoor air conditions were about 20–22 °C, 26–35% RH, 4.7–5.1 g_w/kg_a. The outdoor conditions were −3 to −7 °C, 50 - 65% RH, 1.2 - 1.7 g_w/kg_a. The present theoretical model was run for air flow rates from 0 to 20 CFM. A maximum flow rate, 20 CFM was chosen to keep the air flow in the laminar flow regime to be able to compare with the theoretical model as well as mechanical strength concerns of the sorbent discs.

Performance of SERV in terms of ε_L, VCOP and MRC* for air flow rates varying up to 20 CFM is shown in Fig. 9. As expected, at higher flow rates, the amount of water vapor that could be captured from the air is higher. Therefore, the sorbent discs can capture more water vapor resulting in an increase in MRC*. However, the increase in water uptake is less than the increase in the total amount of water vapor in the air at higher flow rates. Therefore, both latent effectiveness and VCOP have a decreasing trend.

5.2. Cycle time variation

SERV is an intermittently operated device and operates sequentially, equally timed inhale and exhale periods. Effect of half cycle time ranging from 30 s to 300 s was studied. In all the tests, the indoor air conditions were about 21–22 °C, 27–32% RH, 4.6–5.5 g_w/kg_a. The outdoor conditions were −4 to −8 °C, 50 - 60% RH, 1.1 - 1.4 g_w/kg_a.

For all the studied flow rates, the highest performance was achieved at a shorter cycle time as shown in Fig. 10. At the beginning of the inhale or exhale period, the vapor pressure difference between the air and sorbent is the highest. As the half cycle time increases the vapor pressure difference between the air and sorbent decreases that reduces the mass transfer rate. Therefore, a SERV operating with shorter cycle time has a higher mass transfer rate. As the cycle time increases MRC* decrease and eventually reaches a plateau. The latent effectiveness and VCOP have similar decreasing trend with increasing cycle time.

6. Outdoor temperature variation

A set of experiments were performed at outdoor temperatures −21 °C to 9.6 °C, with the outdoor specific humidity ranging from

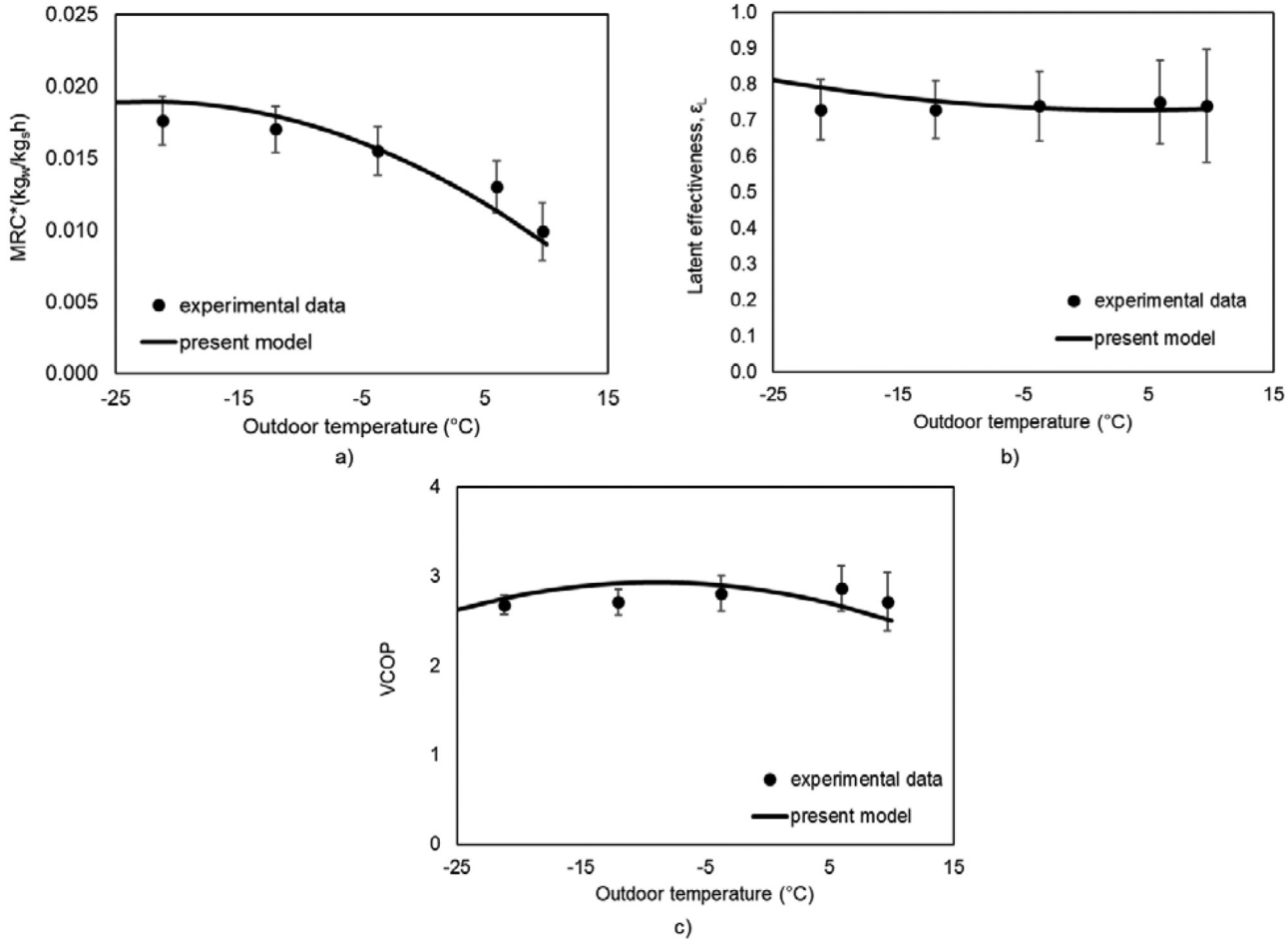

Fig. 11. Performance of the SERV at various outdoor temperatures a) MRC*, b) ε_L, c) VCOP.

1.4 to 3.2 g_w/kg_a accordingly. The air flow rate was constant at about 8 CFM for all the tests.

The performance of SERV at several winter outdoor conditions, −20 °C to 10 °C corresponding to specific humidity of 1.4 g_w/kg_a to 3.2 g_w/kg_a are shown in Fig. 11. The MRC* increases with a decrease in outdoor temperature. The specific humidity of the air decreases when the temperature decreases, therefore the humidity gap between indoor and outdoor enlarges, causing a higher need for humidity recovery. The ε_L and VCOP are a function of the humidity gap; therefore, the increase in the uptake does not affect latent effectiveness and VCOP significantly. The outdoor air condition variation analysis shows that SERV can operate at several different climates without significant deviation in the performance.

7. Comparison with a packed bed system

The proof of concept SERV system comprised of air channeled sorbent discs bed compared with a similar system based on a packed bed, called VENTIREG, made of alumina oxide impregnated with $CaCl_2$ ($Al_2O_3/CaCl_2$ (IK-011–1)) that was built and tested in Russia by Aristov et al. [14]. The packed bed of $Al_2O_3/CaCl_2$ (IK-011–1) with cylindrical pellets, 1.8 mm in diameter and 6 mm in length; ~3 kg in total was tested for air flow rates ranging from 3 to 18 CFM.

The humid indoor air conditions were 20–22 °C, 27–30%RH, dry outdoor air conditions were 17–20 °C, 1.0–1.4%RH. The indoor and outdoor conditions of the present experiment differ from the conditions tested by Aristov et al. [14], however, the specific humidity difference between indoor and outdoor air conditions was similar (4.2–4.6 g_w/kg_a). The performance parameter, β, defines the humidification rate per the available humidity in the RA [14]. Whereas, the latent effectiveness ε_L, defines the dehumidification rate per the humidity gap between indoor and outdoor air. Therefore, the latent effectiveness ε_L, would be a more fair performance indicator to compare the present work with [14].

The performance of the sorbent discs (SERV) is compared to the packed bed of $Al_2O_3/CaCl_2$ (IK-011–1) (VENTIREG) previously reported by Aristov et al. [14]. At flow rates ranging from 3 to 18 CFM, both sorbent beds have similar ε_L and VCOP performance as shown in Fig. 12a-b. As noted, in the present work the indoor and outdoor air conditions are not the same as the conditions of the VENTIREG test. As expected, the performance of the SERV is poorer than VENTIREG in terms of β. Further improvements on the testbed would be a valuable future work to be able to compare the systems at the same indoor and outdoor air conditions.

The compactness of the systems can be better compared using MRC*; sorbent disc design (SERV) has 2.1 kg active material compared with the 3 kg packed bed of $Al_2O_3/CaCl_2$ (IK-011–1). As shown in Fig. 12c-d, the MRC* of sorbent discs (SERV) is up to 30% higher than that of the packed bed (VENTIREG) of $Al_2O_3/CaCl_2$ (IK-011–1). It means that sorbent discs have similar water sorption performance as indicated by ε_L; however, the sorbent discs design is more compact with about 30% less sorbent mass. Considering a 50 to 70% lower pressure drop as shown in Fig. 12d. It can be concluded that the proposed SERV air channeled sorbent discs is

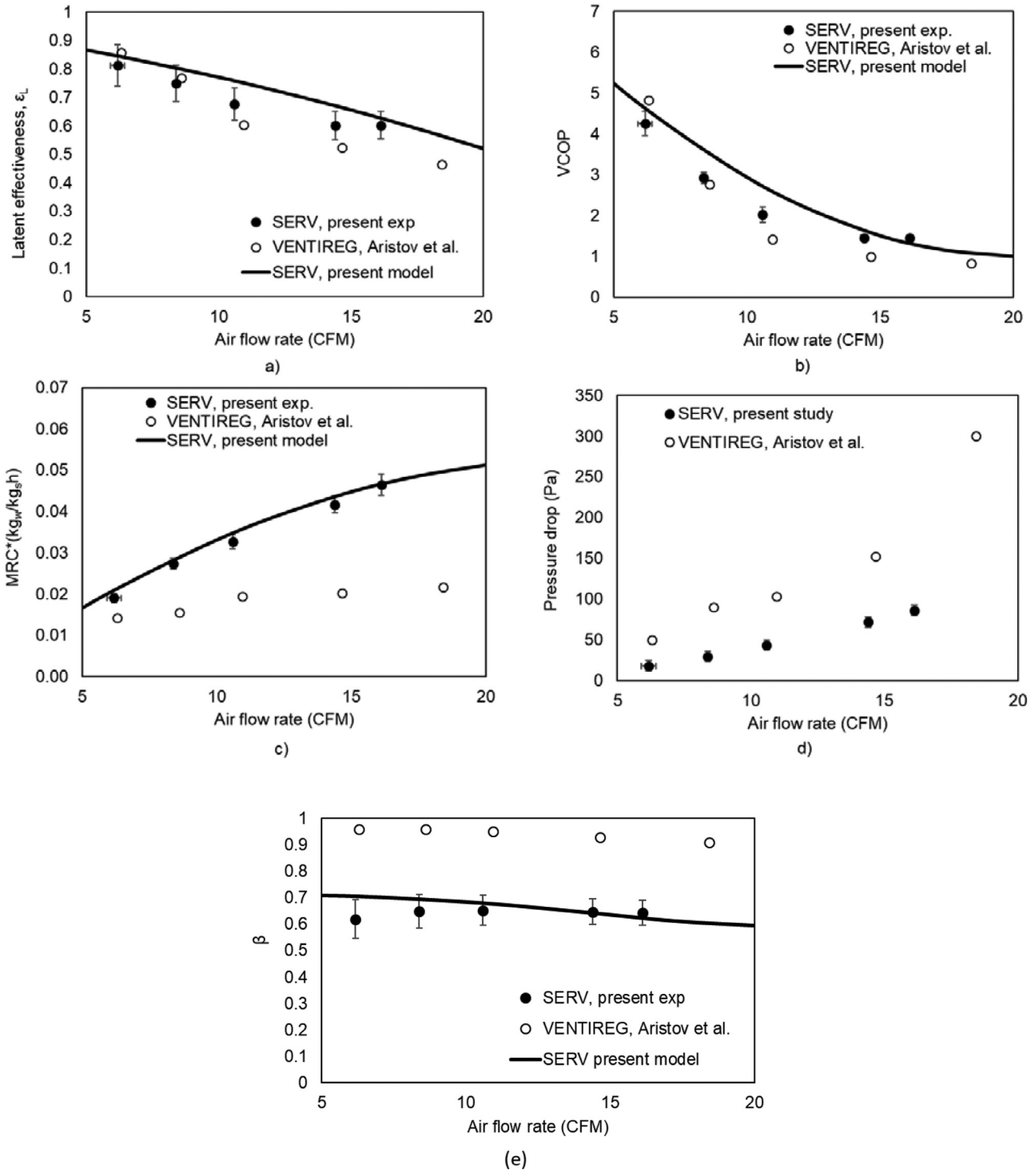

Fig. 12. Performance matrices of the proposed SERV compared against packed bed design (VENTIREG) by Aristov et al. [4].

a promising design for a scaled-up system that requires less fan power.

8. Conclusion

A proof of concept for an air-channeled, disc type sorbent enthalpy recovery ventilation system (SERV) was proposed as a potential replacement for pertinent heat or enthalpy recovery ventilators (HRV/ERV) that require defrosting mechanisms. A theoretical model for heat and mass transfer in air channels of sorbent discs was developed to design the proposed SERV. The air-channeled sorbent discs were built and tested at several different air flow rates, cycle times, and outdoor air conditions down to −15 °C. For the tested conditions, the sorbent discs based SERV can recover up to 70% of the heat and 80% of the moisture, being in a similar range compared to the packed bed system VENTIREG. However, the SERV offers a 60% less pressure drop and 30% less active material.

Author statement

Ecem Cerrah contributed to the manuscript by setting and applying the methodology, mathematical analysis, building the experimental set-up, performing the experiments, data analysis, validation and writing-original draft, review and editing.

We wish to confirm that Dr. Claire McCague has been added as an author during revision process. She helped this manuscript to improve by adding data on material properties, reviewing the experimental data, writing, reviewing editing.

Dr. Majid Bahrami contributed to the manuscript by funding acquisition, setting the methodology, supervision, project administration, writing, review and editing the original draft and revised manuscript.

Declaration of Competing Interest

We wish to confirm that there are no conflicts of interest associated with this publication. Furthermore, we confirm that the manuscript has been read and approved by all the authors whose names are listed in the following. Moreover, we verify that the order of authors listed in the manuscript has been approved by all the authors.

Acknowledgement

The authors gratefully acknowledge the financial support of the Natural Sciences and Engineering Research Council of Canada (NSERC), (RGPIN-2017–03927) and (CUI2I 501951–2016).

Supplementary materials

Supplementary material associated with this article can be found, in the online version, at doi:10.1016/j.enbuild.2020.109755.

References

[1] R. Pichs-Madruga, Y. Sokona, J.C. Minx, E. Farahani, S. Kadner, K. Seyboth, A. Adler, I. Baum, S. Brunner, J. Savolainen, W. Manager, and S. Schlömer, “Climate change 2014 mitigation of climate change summary for policymakers technical summary part of the working group iii contribution to the fifth assessment report of the intergovernmental panel on climate change,” 2015.
[2] P. Nejat, F. Jomehzadeh, M.M. Taheri, M. Gohari, M.Z. Abd. Majid, A global review of energy consumption, CO2 emissions and policy in the residential sector (with an overview of the top ten CO2 emitting countries), Renew. Sustain. Energy Rev. 43 (Mar. 2015) 843–862.
[3] International Energy Agency, “Energy technology perspectives 2016,” 2016.
[4] “Residential sector canada table 2: secondary energy use and GHG emissions by end-use | natural resources canada.” [Online]. Available:http://oee.nrcan.gc.ca/corporate/statistics/neud/dpa/showTable.cfm?type=CP&sector=res&juris=ca&rn=2&page=4. [Accessed: 14-Feb-2019].
[5] I. - International Energy Agency, “Insights series 2018: energy efficiency potential in Canada.”
[6] ASHRAE, ASHRAE 62.1-2015 ventilation for acceptable indoor air quality, Am. Soc. Heat. Refrig. Air Cond. Eng. (2015).
[7] ATTMA, Technical standard L1 - measuring air permeability of building envelopes, Air Tightness Test. Meas. Assoc. (2010).
[8] B. of B. H. Homeowner Protection Office, “Heat recovery ventilation guide for houses,” 2015.
[9] A. Mardiana-Idayu, S.B. Riffat, Review on heat recovery technologies for building applications, Renew. Sustain. Energy Rev. 16 (2) (Feb. 2012) 1241–1255.
[10] R. Ahmed, J. Appelhoff, Frost-protection measures in energy recuperation with multiple counterflow heat exchangers, Rehva 05 (October) (2013) 37–40.
[11] C. Beattie, P. Fazio, R. Zmeureanu, J. Rao, Experimental study of air-to-air heat exchangers for use in arctic housing, Appl. Therm. Eng. 129 (2018) 1281–1291.
[12] P. Liu, M. Justo Alonso, H.M. Mathisen, C. Simonson, Energy transfer and energy saving potentials of air-to-air membrane energy exchanger for ventilation in cold climates, Energy Build. 135 (Jan. 2017) 95–108.
[13] Y.I. Aristov, I.V. Mezentsev, V.A. Mukhin, A new approach to regenerating heat and moisture in ventilation systems, Energy Build. 40 (3) (2008) 204–208.
[14] Y.I. Aristov, I.V. Mezentsev, V.A. Mukhin, Investigation of the moisture exchange in a stationary adsorbent layer through which air is passed, J. Eng. Phys. Thermophys. 78 (2) (2005) 44–50.
[15] R.E. Hayes, Forced convection heat transfer at the boundary layer of a packed bed, Transp. Porous Media 5 (3) (1990) 231–245.
[16] F. Incropera, D. DeWitt, T. Bergrnan, *Fundamentals of Heat and Mass Transfer*, 6th ed., 2007.
[17] M. Ahmadi, M.F. Pakdaman, M. Bahrami, Pushing the limits of vertical naturally-cooled heatsinks; calculations and design methodology, Int. J. Heat Mass Transf. 87 (2015) 11–23.
[18] M. Friedlander, G.M. Dobbs, B.N. Erb, M.W. Foster, C. Garcia, R.R. Moffitt, K.B. Peck, C.J. Simonson, K.W. Cooper, W.F. Walter, D.S. Abramson, C.S. Barnaby, S.J. Emmerich, J.M. Ferguson, R.L. Hall, and R.M. Harrold, “ANSI/ ASHRAE standard 84 -2013 method of testing air-to-air heat / energy exchangers,” Atlanta/ USA, 2013.
[19] R. Narayanan, W.Y. Saman, S.D. White, M. Goldsworthy, Comparative study of different desiccant wheel designs, Appl. Therm. Eng. 31 (10) (2011) 1613–1620.
[20] C.R. Ruivo, J.J. Costa, A.R. Figueiredo, On the validity of lumped capacitance approaches for the numerical prediction of heat and mass transfer in desiccant airflow systems, Int. J. Therm. Sci. 47 (3) (2008) 282–292.
[21] C.J. Simonson, R.W. Besant, Heat and moisture transfer in desiccant coated rotary energy exchangers : part i . numerical model, HVAC&R Res. 3 (4) (1997) 325–350.
[22] G. Angrisani, C. Roselli, M. Sasso, Effect of rotational speed on the performances of a desiccant wheel, Appl. Energy 104 (2013) 268–275.
[23] S. De Antonellis, C.M. Joppolo, L. Molinaroli, Simulation, performance analysis and optimization of desiccant wheels, Energy Build. 42 (9) (2010) 1386–1393.
[24] C.X. Jia, Y.J. Dai, J.Y. Wu, R.Z. Wang, Use of compound desiccant to develop high performance desiccant cooling system, Int. J. Refrig. 30 (2) (2007) 345–353.
[25] X.J. Zhang, Y.J. Dai, R.Z. Wang, A simulation study of heat and mass transfer in a honeycombed rotary desiccant dehumidifier, Appl. Therm. Eng. 23 (8) (2003) 989–1003.
[26] L.A. Sphaier, W.M. Worek, Analysis of heat and mass transfer in porous sorbents used in rotary regenerators, Int. J. Heat Mass Transf. 47 (14–16) (2004) 3415–3430.
[27] L. Yadav, A. Yadav, Mathematical investigation of purge sector angle for clockwise and anticlockwise rotation of desiccant wheel, Appl. Therm. Eng. 93 (2016) 839–848.
[28] Y.S. Muzychka, M.M. Yovanovich, Laminar forced convection heat transfer in the combined entry region of non-circular ducts, J. Heat Transf. 126 (1) (2004) 54.
[29] Y.S. M. and M.M. Yovanovich, “Modeling nusselt numbers for thermally developing laminar flow in non-circular ducts,” 1998.
[30] J.P. Holman, Heat Transf. (2010) Tenth.
[31] E. Cerrah, Sorbent Based Enthalpy Recovery Ventilator (SERV) in Northern Building Applications, Simon Fraser University, 2019.